AN ENGINEERING APPROACH TO THE CALCULATION OF TWO-AND-THREE DIMENSIONAL FLOWS WITH EXTENSIVE SEPARATION

Tuncer Cebeci, Forrester Johnson, K. C. Chang and H. H. Chen
The Boeing Company, Long Beach, CA

Keywords: *Aerodynamics, high lift flows, and separation*

Abstract

A calculation method for predicting the performance of airfoils, multi-element airfoils, wings and multi-element wings based on an interactive boundary-layer approach using an improved Cebeci-Smith turbulence model is described. Inviscid flow solutions based on panel and full-potential methods are coupled to an inverse finite difference method using Veldman's interaction law. Results are presented for single and multi-element airfoil as well as single and multi-element wing configurations. Overall calculated results show very good agreement with experiments..

1 Introduction

In recent years significant progress has been made to accurately compute aerodynamic flows. Modern methods for solving the Navier-Stokes equations have been developed and applied to calculate aerodynamic performance of complex configurations, including the whole aircraft, for a wide range of flow conditions. In addition, several interactive boundary-layer methods to couple the solutions of inviscid and boundary-layer equations have been developed for the same purpose. Despite this progress, however, our ability to calculate separated flows is still in its infancy. The calculation of important flow characteristics of wings and high lift systems near stall and post stall is still not satisfactory.

The study reported here deals with improving our ability to calculate separated flows. It is based on the interactive boundary-layer method developed by Cebeci. Reference 1 describes the theory and its applications to a wide range of steady and unsteady subsonic two-dimensional and steady subsonic three-dimensional flows. In all cases, the inviscid flow is calculated by the Hess panel method[1]. The interactive boundary-layer method has also been applied to steady two- and three-dimensional transonic flows. This approach, however, has not been as thorough as the one for subsonic flows. In all cases, the studies show that the lift and drag characteristics of airfoils, wings and high lift systems can be predicted efficiently and accurately for a wide range of flow conditions, including flows with extensive separation.

The present study deals with the calculation of airfoil characteristics at low Mach numbers. While the previous studies on this subject used a panel method [1], this study uses the TRANAIR code [2] and is conducted as a prelude to its application to three-dimensional flows. The next section presents a brief description of the interactive boundary-layer approach for incompressible flows. Results are given in the following section (Section 3.0) for a sample of airfoils in order to demonstrate the accuracy of the calculation method. In sections 4, 5 and 6 results are given for two-dimensional high lift systems, wings and three-dimensional high lift systems, obtained with the Hess panel method and interactive boundary-layer method. The paper ends with a summary of more important conclusions and plans for work in progress.

2 Description of the Calculation Method

To calculate subsonic flows over airfoils, at first an inviscid velocity distribution is obtained for

the given airfoil geometry and flow conditions. The boundary-layer equations are solved in the inverse mode with transition determined by the e^n-method or Michel's criteria. The blowing velocity distribution, $\upsilon_b(x)$, and the displacement thickness on the airfoil and in the wake, are then used to obtain an improved inviscid velocity distribution with viscous effects. The displacement thickness at the trailing edge is used to satisfy the Kutta condition at a distance equal to δ^*_{te}. In the second iteration between the inviscid and inverse boundary-layer methods, $\upsilon_b(x)$ is used to replace the zero blowing velocity at the surface. At the next and following iterations, the difference in $\upsilon_b(x)$ between iterations is added to the previous blowing velocity used as a boundary condition in the inviscid method. This procedure is repeated for several cycles until convergence based on the lift and total drag coefficients of the airfoil is obtained. Studies show that, in general, with three boundary-layer sweeps for one cycle, convergence is obtained in less than 10 cycles. For additional details, see Reference 1.

2.1 Inverse Boundary-Layer Method

The inverse boundary-layer (IBL) method is a differential method based on the solutions of the continuity and momentum equations solved by a two-point finite-difference method. These equations, using an eddy viscosity (ε_m) concept for the Reynolds shear stress, can be written as

$$\frac{\partial u}{\partial x}+\frac{\partial \upsilon}{\partial y}=0 \qquad (1)$$

$$u\frac{\partial u}{\partial x}+\upsilon\frac{\partial u}{\partial y}=u_e\frac{du_e}{dx}+\frac{\partial}{\partial y}\left(b\frac{\partial u}{\partial y}\right) \qquad (2)$$

where

$$b=\nu+\varepsilon_m \qquad (3)$$

In the absence of mass transfer, the boundary conditions on the airfoil are

$$y=0;\quad u=0,\quad \upsilon=0 \qquad (4a)$$

$$y=\delta;\quad u=u_e \qquad (4b)$$

In the wake, where a dividing line at $y = 0$ is required to separate the upper and lower parts of the inviscid flow, the boundary conditions are

$$y=0;\quad \upsilon=0,\quad \frac{\partial u}{\partial y}=0 \qquad (5)$$

2.2 Solution Procedure

The solutions of the above system are obtained by first expressing the equations in transformed coordinates. Two sets of transformed coordinates are used, one for the direct problem when the equations are solved for the prescribed pressure distribution, and the other for the inverse problem with the external velocity updated during the iterations. Falkner-Skan transformation is used in the direct mode and the modified transformation in the inverse mode. The airfoil is divided into upper and lower surfaces. For each surface, the calculations start at the stagnation point and proceed in standard mode up to a certain specified location. Then, the inverse calculations are performed from this switch location to the far wake. For details, see [1].

2.3 Interaction Law

To couple the inviscid and viscous flow solutions, an interaction law due to Veldman is used. According to this law, the external velocity is represented by

$$u_e(x)=u_e^o(x)+\delta u_e(x) \qquad (6)$$

where u_e^o is the inviscid velocity computed by the inviscid method and δu_e is the perturbation velocity due to viscous effects, which is given by the Hilbert integral

$$\delta u_e=\frac{1}{\pi}\int_{x_a}^{x_b}\frac{d}{d\sigma}\left(u_e\delta^*\right)\frac{d\sigma}{x-\sigma} \qquad (7)$$

in the interaction region (a, b).

2.4 Turbulence Model

The inverse boundary-layer method uses an improved eddy viscosity formulation of Cebeci and Smith. According to this new formulation, Cebeci and Chang [1] expressed the parameter

α in the outer eddy viscosity formula as a variable related to the ratio of the product of the turbulence energy by normal stresses to the shear stress at the location where the shear stress is maxmium. In addition, the intermittency expression was replaced with the one recommended by Fiedler and Head [1].

3 Results for Four Airfoils

The inverse boundary-layer (IBL) method coupled to TRANAIR was applied to calculate flows over three airfoils and comparisons were made with both the experimental data and previous results obtained with the panel method

Figures 1 to 3 show the results for the NACA 0012 airfoil at a Mach number of 0.3 and a chord Reynolds number of 3.9×10^6. Fig. 1 shows a comparison between the calculated and measured pressure coefficient distributions with for two angles of attack corresponding to $\alpha=12^o$ and 13°, and Fig. 2 shows the results for lift coefficients as a function of angle of attack. As can be seen, the calculated results obtained with the panel method with compressibility corrections and TRANAIR both agree well with measurements and there is practically no difference between results obtained by the two different inviscid methods. Fig. 3 shows the onset of flow separation on the airfoil as a function of angle of attack. The results indicate that there is no flow separation at $\alpha=11^\circ$, but there is about 20% region of flow separation at $\alpha=14.5^\circ$.

Figures 4 to 6 show similar results for the NLR-1 airfoil at a Mach number of 0.3 and a chord Reynolds number of 3.9×10^6. This airfoil is also based on the "peakey" airfoil concept developed by Wortman, combined with an inverse camber built into the trailing-edge region of the airfoil to reduce the pitching moment. Fig. 4 shows comparisons between calculated and measured pressure coefficient distributions at two angles of attack, $\alpha=12^\circ$ and 13.5° and Fig. 5 shows a comparison between measured and calculated lift coefficients. Unlike the results for the previous airfoils, the results of the panel method and TRANAIR become different at higher angles of attack, while they are essentially the same at low and moderate angles of attack. Clearly TRANAIR results are better than those of the panel method near stall. This is because the compressibility corrections used in the panel method do not accurately account for compressibility effects. The results in Fig. 6 indicate that there is about 25% flow separation region on this airfoil at $\alpha=14^\circ$.

Figures 7 and 8 show the results for a Boeing airfoil at a Mach number of 0.201 and a chord Reynolds number of 2.8×10^6. The results shown in Fig. 7 indicate that, as for the Wortman airfoil, the predicted lift coefficients with TRANAIR, while in good agreement at low and moderate angles of attack with those obtained with the panel method, agree much better with measurements at higher angles of attack than those obtained with the panel method. Fig. 8 shows that the maximum flow separation on this airfoil is more than 20% at $\alpha=15.5^\circ$.

The above results show that the coupling of TRANAIR and IBL predicts lift coefficients which are in very good agreement with experimental data for compressible flows at low Mach numbers. The results of TRANAIR + IBL are essentially the same as those obtained with a panel method + IBL at low and moderate angles of attack. At high angles of attack, near stall and past stall, the compressibility corrections used in the panel method do not give consistent results. For flows, for example, where a shock occurs near the leading edge, the results obtained with TRANAIR + IBL are in better agreement with experimental data than those obtained with the panel method + IBL. Results also show that rather large regions of separated flows can be computed with the interactive boundary layer approach using both the panel method and TRANAIR.

While it needs to be demonstrated, it is very likely that the predictions of TRANAIR + IBL, when extended to high lift systems and wings, will be as good, if not better, as those obtained with the panel method + IBL which

has already been successfully extended to such flow configurations. To demonstrate this claim, in the following sections, we present sample results obtained with the panel method + IBL for flows on multi-element airfoils, wings and multi-wings.

4 Applications to Two-Dimensional Incompressible Flows: High Lift Systems

Figures 9 and 10 show results for the NLR 7301 supercritical airfoil/flap configuration. The experimental data of Van den Berg and Oskam include pressure distributions at $\alpha = 6^\circ$ and 13.1°, lift curve and drag polar for the airfoil with a flap of 32% chord deflected at an angle of 20° and with a gap of 2.6% chord. The experimental was conducted with $M_\infty = 0.185$, and a chord Reynolds number of 2.51×10^6. The compressibility corrections used in the panel method are based on the Prandtl-Glauert formula. Fig. 9 shows a comparison between measured and computed pressure distributions at $\alpha = 6^\circ$ and 13.1°, and Fig. 10 shows a comparison of the lift and drag coefficients. The viscous flow calculations were performed with the onset of transition location on the main element and flap calculated. As can be seen from Fig. 10, the calculated results agree well with experimental data.

Figures 11 and 12 show the results for a NASA high lift configuration tested by Omar et al for a free stream Mach number of $M_\infty = 0.201$ and chord Reynolds number of 2.83×10^6. Fig. 11 shows the pressure distributions for the airfoil/flap configuration at $\alpha = 0.01^\circ$ and 8.93° and Fig. 12 shows the lift and drag coefficients for the same configuration. The lift coefficient is slightly over predicted due to the discrepancies on the flap upper surface, and similarly the drag coefficient is slightly under predicted. Also, the calculated incompressible stall angle is rather different from that of the compressible calculations. The critical pressure coefficient for $M_\infty = 0.201$ is indicated in Fig. 11(b). At $\alpha = 8.93^\circ$, the measured stall angle, there exists a small region of supersonic flow and a shock may occur. Even though this shock cannot be predicted by the panel method, the compressibility corrections, theoretically applicable at lower angles of attack only, provide a significant improvement to the stall prediction. However, a compressible flow solver such as TRANAIR should be used to achieve more accurate predictions.

5 Applications to Three-Dimensional Flows: Wing Configurations

The calculation method using the Hess panel method and IBL has also been applied to wing and multi-element wings. A sample of results is presented for the RAE wing tested by Lovell to demonstrate the ability of the method for such flows.

The RAE wing has an airfoil section which has considerable rear loading with the maximum thickness of 11.7% located at 37.5% chord and the maximum camber located at 75% chord. The wing has neither twist nor dihedral, but has a quarter-chord sweep angle of 28° and a taper ratio of $1/4$. Experiments were conducted at a Reynolds number of 1.35×10^6 with measurements corresponding to both free transition and fixed transition for a freestream Mach number of 0.223.

In Lovell's experiments, fix transition was set by using a series of 0.5mm diameter wires positioned streamwise round the leading edge from 10% chord on the upper surface to 10% chord on the lower surface. Ten wires were equally spaced across each half wing. Measurements showed that the maximum lift coefficient with fixed transition is higher than that with free transition. Lovell noted, however, that "a larger portion is probably caused by the tendency of the streamwise wires to act as vortex generators." Also, at post stall conditions, the flow becomes largely unsteady and only average measurements were reported. Therefore, near maximum lift, calculated results with fixed transition should be compared with free transition measurements. Fig. 13 shows the lift and drag coefficient variations with angle of

attack including experimental data with both free and fixed transition. The calculations were performed with 10 uniformly spaced cross-sections along the span, each cross-section being defined by 63 points with a higher point concentration around the leading and the trailing edges. The increment in angle of attack is 2° for angle of attack less than 10^o and is reduced to 1° beyond that point. Results show that with the original Cebeci-Smith (C.S.) turbulence model, the lift coefficient keeps increasing past the measured stall angle (around 12° with free transition). For the modified C.S. turbulence model, on the other hand, the agreement between measured and calculated lift coefficient is excellent up to 14°. At 15°, the boundary layer calculations at η_b = 0.7 do not converge near the trailing edge due to rather large separated flow region. Fig. 14 shows the onset of flow separation along the span for two angles of attack. As can be seen, rather large separated flows can be calculated with this method

6 Applications to Three-Dimensional Flows: High Lift Systems

The calculation method has also been applied to several high lift configurations of the RAE wing. The full-span slat is either retracted or deployed at 25° and the full span flap is deployed at either 10° or 25°.

The cross-section of the wing-flap configuration with the flap deflected at 10° is shown in Fig. 15(a). The lift coefficient variation with angle of attack and the drag polar are also shown in Fig. 15. The lift coefficient for inviscid flow is included to show how the introduction of viscous effects allows for a better prediction of the lift curve. However, the lift coefficient is over-predicted while the drag coefficients, except near stall, are well predicted. From Fig. 15(a), it can be seen that the flap is positioned very close to the main element. Therefore, merging of the main element wake with the boundary layer developing on the flap upper surface is likely to occur. This merging, observed in two-dimensional flows, may be the source of the discrepancy since it is not modeled in the present method.

Fig. 16 shows the results when the flap is deflected at 25°. Observations similar to those of the previous paragraph can be made. Agreement between measurements and calculations is satisfactory for both lift and drag coefficient. As expected, the larger flap deflection (25° instead of 10°) causes a larger difference between inviscid and viscous flow calculations.

Fig. 17 shows results for the RAE wing with slat deflected at 25° and flap deflected at 10° and Fig. 18 shows similar results when both slat and flap are deflected at 25°. Again, the lift coefficient for inviscid flow is included to show how the viscous flow calculation improves predictions of lift and drag coefficients. As can be seen, the interactive boundary-layer method predicts the lift and drag coefficients quite well.

7 Recommendations

The studies conducted so far indicate that the use of IBL is an excellent approach to incorporate separated flow analysis in TRANAIR. It is clear that what has already been achieved with a panel method can also be achieved with TRANAIR. As a matter of fact, preliminary studies conducted for low Mach numbers indicate that the use of TRANAIR with IBL will allow the calculation of larger regions of flow separation than those achieved with a panel method + IBL. For example, our calculations for the NACA 0012 airfoil indicate that results can be obtained without any difficulties and substantial flow separation over 65% of the chord length can be predicted.

Our current studies with TRANAIR on high lift systems for two-dimensional flows also indicate good agreement with experimental data. As expected the results with TRANAIR agree well with those of panel method at low and moderate angles of attack. However, at high angles of attack, especially near stall, the prediction of the calculation method with TRANAIR is much better.

References

[1] Cebeci, T. *An engineering approach to the calculation of aerodynamic flows*. to be published by Springer-Verlag, 1998.

[2] TRANAIR user's manual, version D00. 1994.

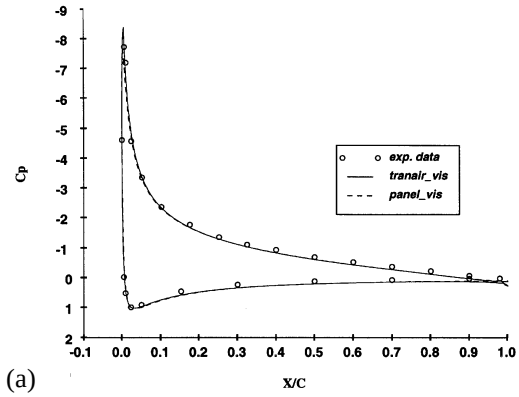

(a)

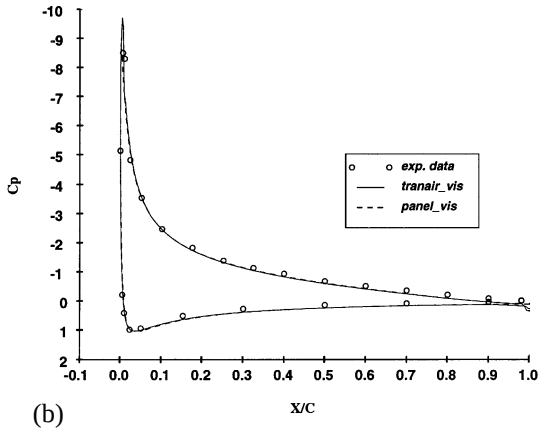

(b)

Fig. 1. Comparison of calculated and measured pressure coefficient distributions for the NACA 0012 airfoil at $M_\infty = 0.3, R_c = 3.9\times10^6$, (a) $\alpha = 12^\circ$, (b) $\alpha = 13^\circ$

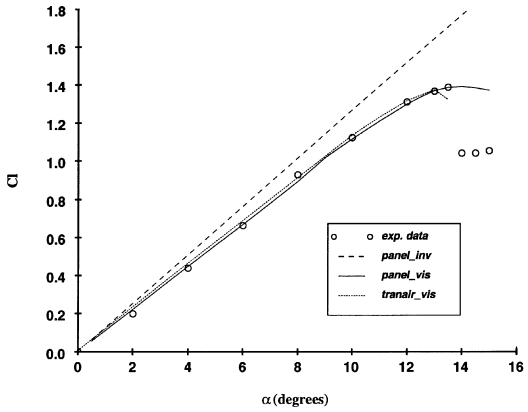

Fig. 2. Comparison of calculated lift coefficients with experimental data for the NACA 0012 airfoil at $M_\infty = 0.3, R_c = 3.9\times10^6$

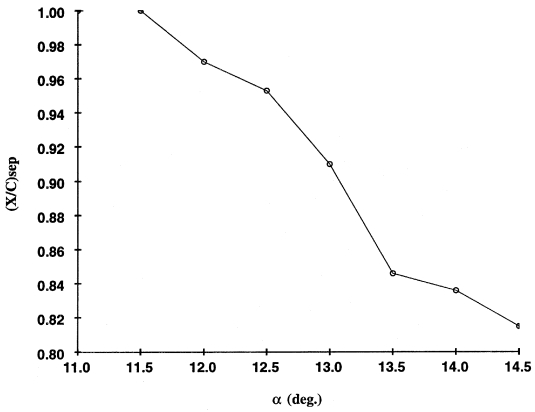

Fig. 3. Flow separation on the NACA 0012 airfoil at different angles of attack with $M_\infty = 0.3, R_c = 3.9\times10^6$

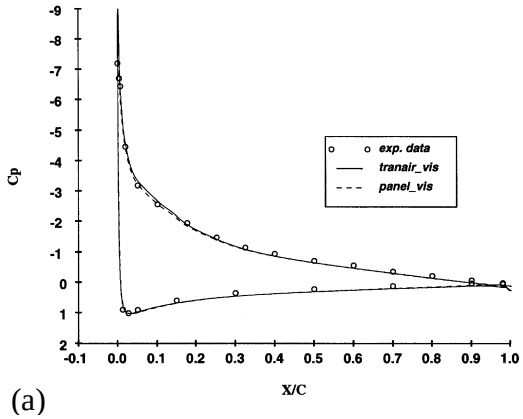

(a)

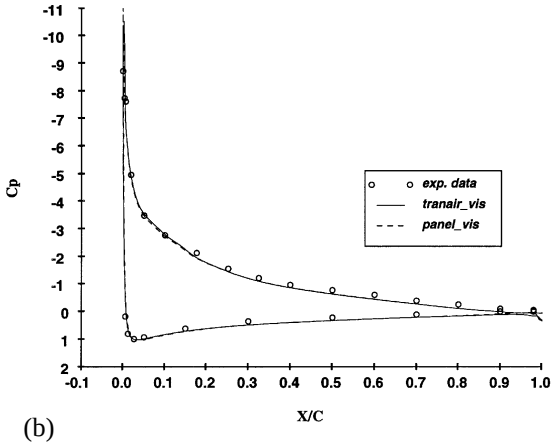

(b)

Fig. 4. Comparison of calculated and measured pressure coefficient distributions for the Wortman airfoil at $M_\infty = 0.3, R_c = 3.9\times10^6$, (a) $\alpha = 12^\circ$, (b) $\alpha = 13.5^\circ$

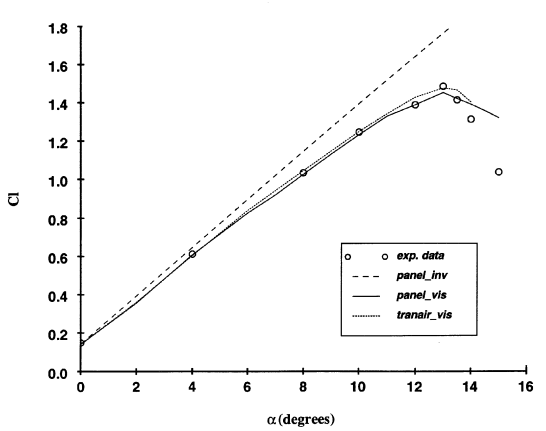

Fig. 5. Comparison of calculated lift coefficients with experimental data for the Wortman airfoil at $M_\infty = 0.3, R_c = 3.9\times10^6$

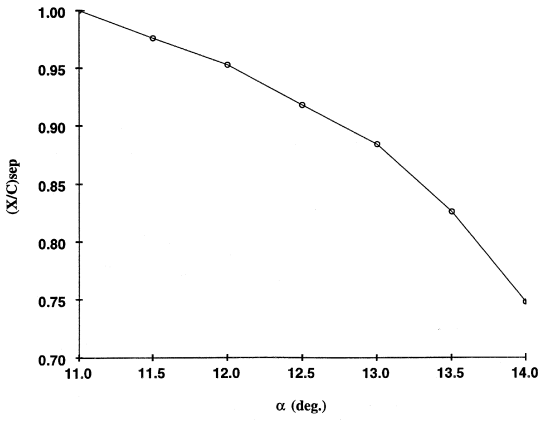

Fig. 6. Flow separation on the Wortman airfoil at different angles of attack with $M_\infty = 0.3, R_c = 3.9\times10^6$

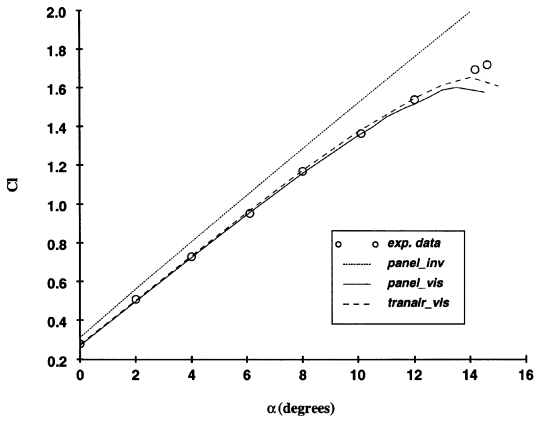

Fig. 7. Comparison of calculated lift coefficients with experimental data for the Boeing airfoil at $M_\infty = 0.201, R_c = 2.8\times10^6$

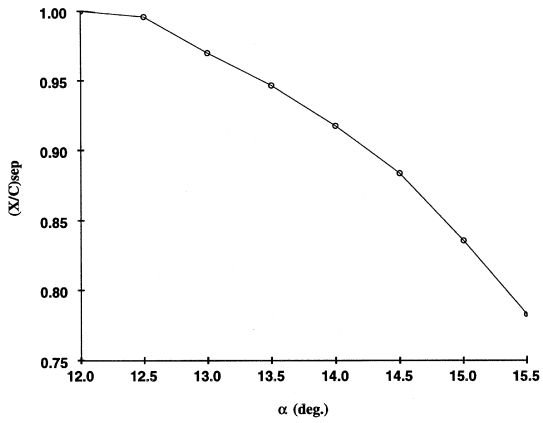

Fig. 8. Flow separation on the Boeing airfoil at different angles of attack with $M_\infty = 0.201, R_c = 2.8\times10^6$

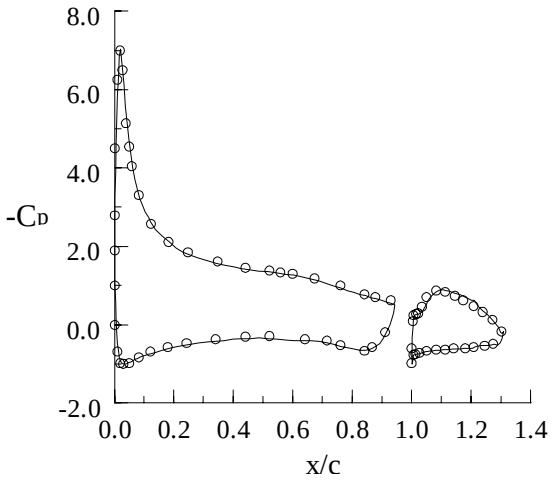

(a)

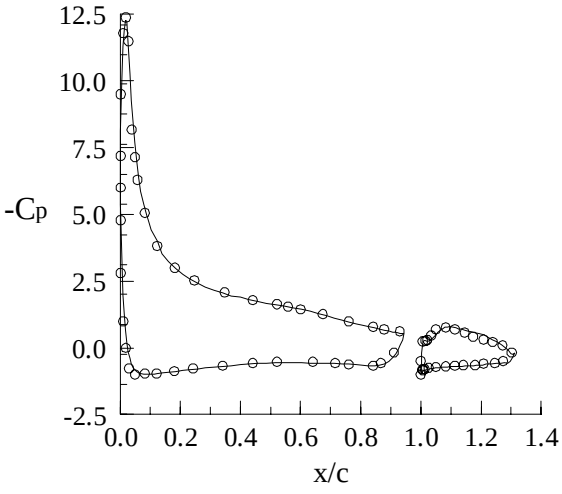

(b)

Fig. 9. Comparison of measured (symbols) and calculated (continuous lines) pressure distributions for the NLR 7301 supercritical airfoil/flap configuration for (a) $\alpha = 6^{\circ}$ and (b) $\alpha = 13.1^{\circ}$.

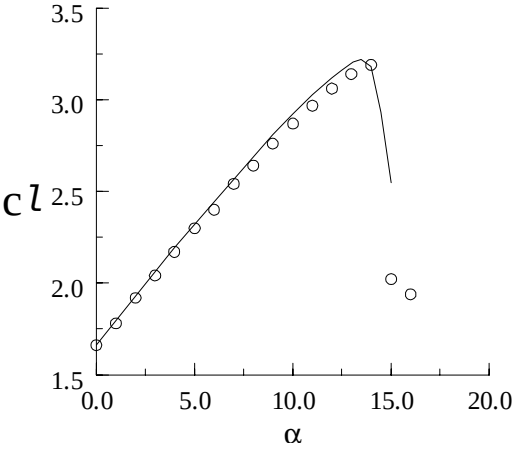

(a)

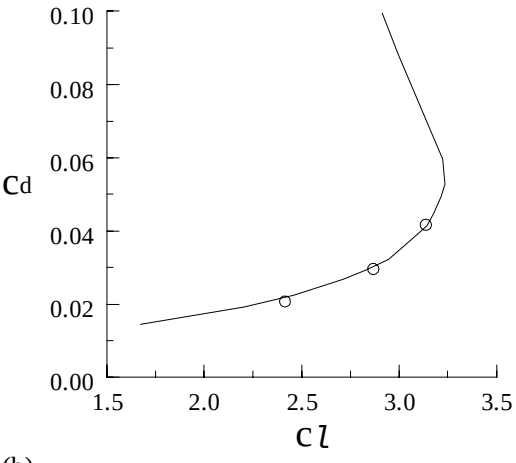

(b)

Fig. 10. Comparison of measured (symbols) and calculated (continuous lines) (a) lift and (b) drag coefficients for the NLR 7301 supercritical airfoil/flap configuration

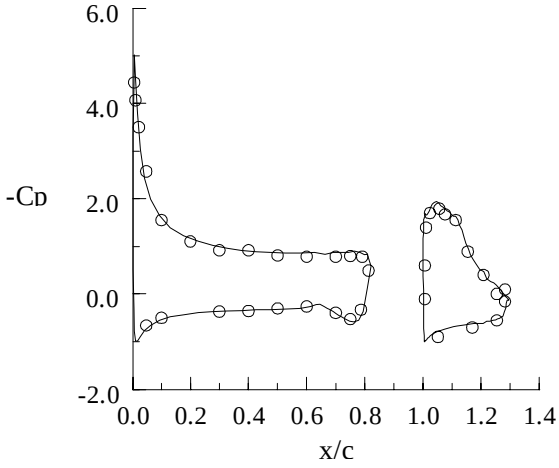

(a)

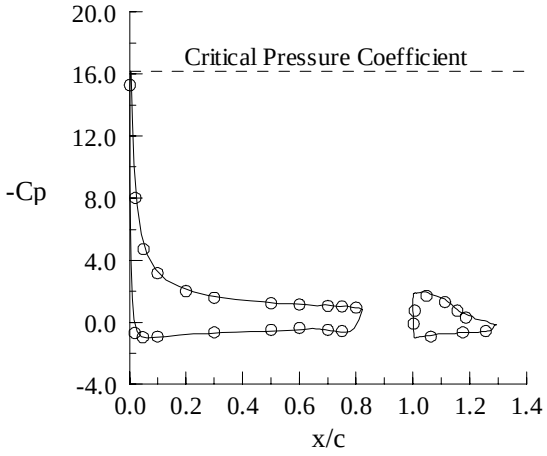

(b)

Fig. 11. Comparison of measured (symbols) and calculated (continuous lines) pressure distributions for the NASA airfoil/flap configuration at (a) $\alpha = 0.01^{\circ}$ and (b) $\alpha = 8.93^{\circ}$.

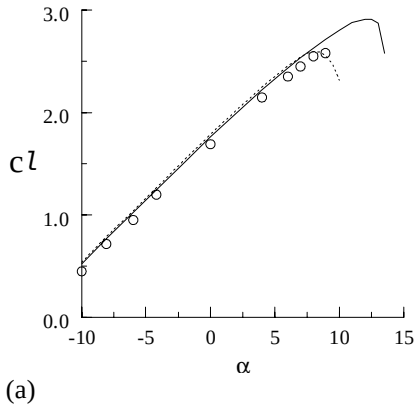

(a)

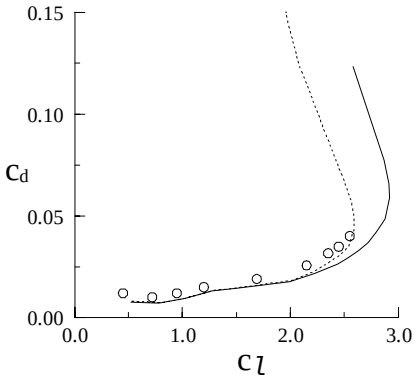

(b)

Fig. 12. Comparison of measured (symbols) and calculated (lines) (a) lift coefficients, and (b) drag polars for the NASA airfoil/flap configuration. Continuous lines denote incompressible calculations and dotted lines compressible calculations

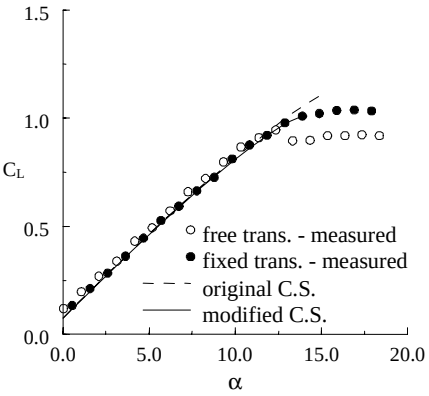

(a)

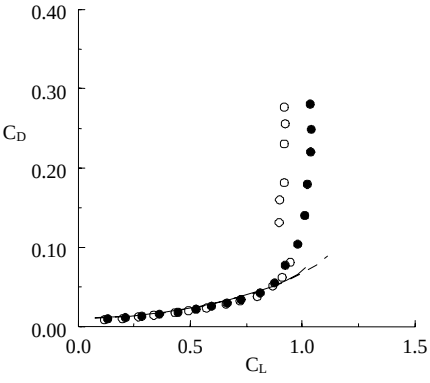

(b)

Fig. 13. Single wing: Effect of turbulence model on (a) lift and (b) drag coefficients

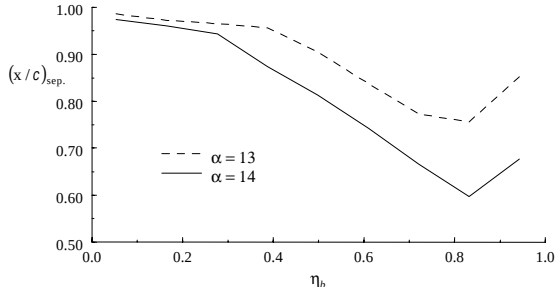

Fig. 14 Distribution of flow separation along the span at two angles of attack

(a)

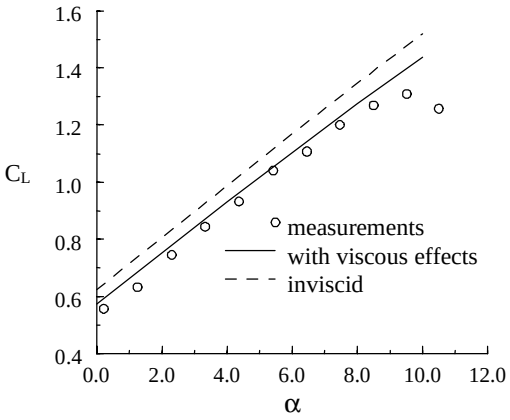

(b)

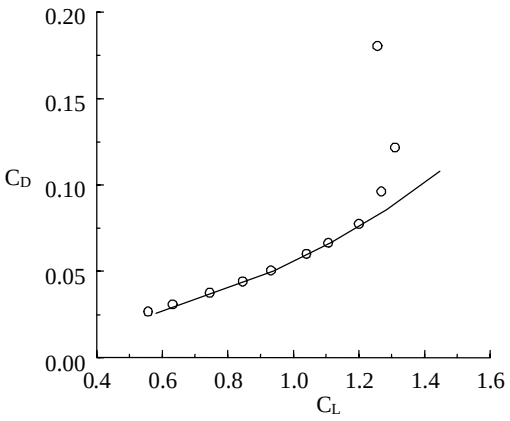

(c)

Fig. 15. RAE wing with slat retracted and flap deflected at 10^{o}, (a) wing cross-section, (b) lift coefficient, and (c) drag coefficient.

(a)

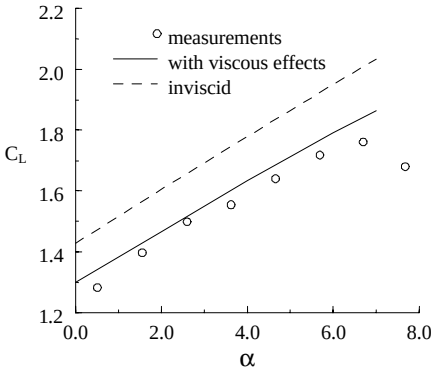

(b)

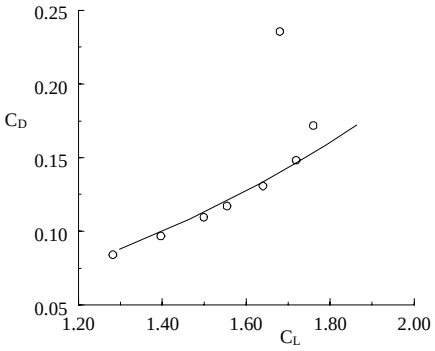

(c)

Fig. 16. RAE wing with slat retracted and flap deflected at 25°, (a) wing cross-section, (b) lift coefficient, and (c) drag coefficient.

(a)

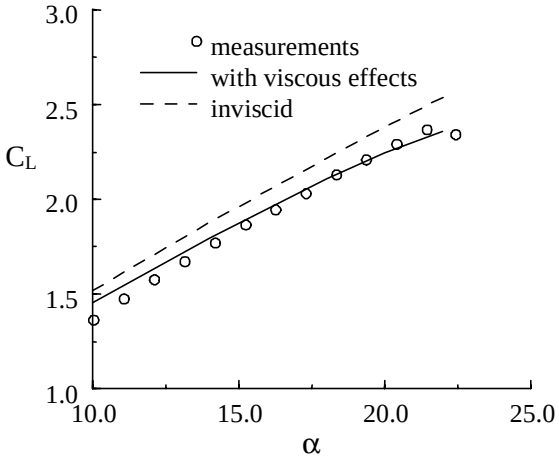

(b)

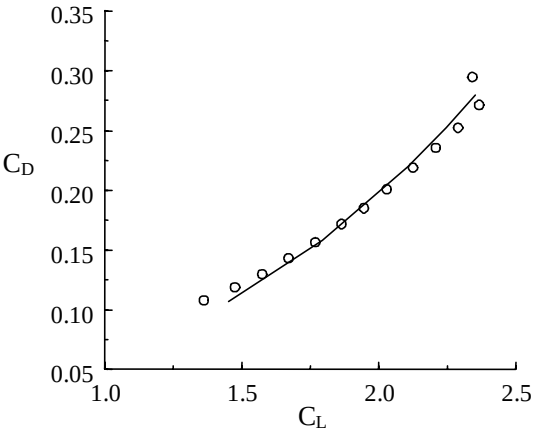

(c)

Fig. 17. RAE wing with slat deflected at 25° and flap deflected at 10°, (a) wing cross-section, (b) lift coefficient, and (c) drag coefficient.

(a)

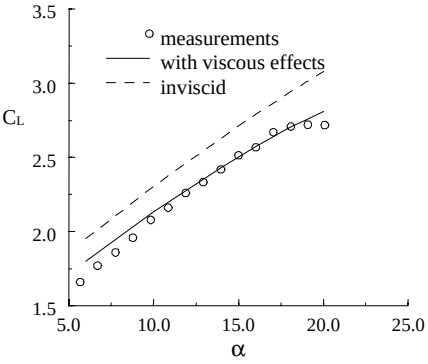

(b)

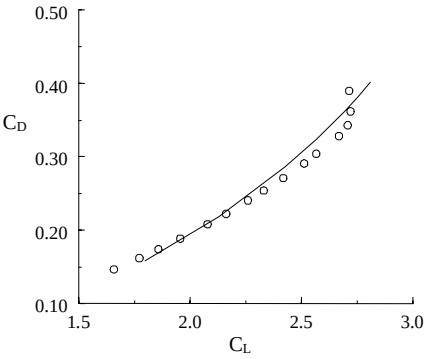

(c)

Fig. 18. RAE wing with both slat and flap deflected at 25°, (a) wing cross-section, (b) lift coefficient, and (c) drag coefficient.